Enhanced binding of guanylated poly(A) RNA by the LaM domain of LARP1

Guennadi Kozlov[1,2], Jianning Jiang[1,2], Tyler Rutherford[3], Anne M. Noronha[3], Christopher J. Wilds[3], Kalle Gehring[1,2,*]

[1]Department of Biochemistry, McGill University, Montréal, Canada

[2]*Centre de recherche en biologie structurale*, McGill University, Montréal, Canada

[3]Department of Chemistry and Biochemistry, Concordia University, Montréal, Canada

*Corresponding author: kalle.gehring@mcgill.ca

Keywords: LaM, La motif; LARP, La-related protein; LARP1, La-related protein 1; poly(A) tail; guanylation; phosphorothioate

ABSTRACT

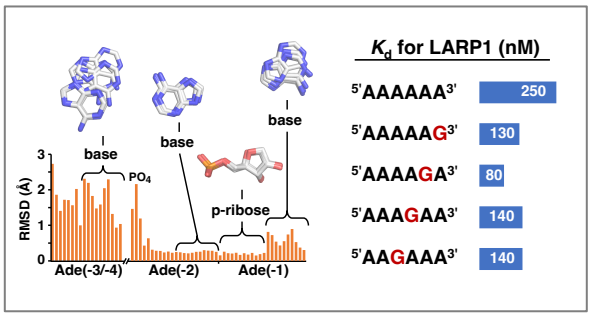

La-related proteins (LARPs) are a family of RNA-binding proteins that share a conserved La motif (LaM) domain. LARP1 plays a role in regulating ribosomal protein synthesis and stabilizing mRNAs and has a unique structure without an RNA binding RRM domain adjoining the LaM domain. In this study, we investigated the physical basis for LARP1 specificity for poly(A) sequences and observed an unexpected bias for sequences with single guanine substitutions. Remarkably, multiple guanine substitutions did not further increase binding affinity, demonstrating preferential recognition of singly guanylated sequences. Affinity measurements were complemented by high-resolution crystal structures of the LARP1 LaM with six different RNA ligands, including two stereoisomers of a phosphorothioate linkage. The selectivity for singly substituted poly(A) sequences suggests LARP1 plays a role in the stabilizing effect of poly(A) tail guanylation, while the plasticity in base recognition underlines the importance of the ribose 3´-terminus for RNA binding.

INTRODUCTION

La-related protein 1 (LARP1) is a member of the LARP family of RNA-binding proteins that includes LARP1B, LARP3 (genuine La protein), LARP4, LARP4B, LARP6, and LARP7. Each member has distinct functional roles in RNA metabolism and gene expression regulation [1, 2]. All LARPs share a highly conserved La motif (LaM) domain, which is generally accompanied by a downstream RNA recognition motif (RRM) [3, 4]. This tandem arrangement constitutes the La-module [5, 6]. Among human proteins, LARP1 and the related LARP1B are the only members that do not possess the RRM domain [7]. Instead, the region following the LaM domain contains a PAM2 motif (PABP-interacting motif 2), which binds poly(A)-binding protein C1 (PABPC1) [2]. The other well-characterized domain in LARP1 is the C-terminal DM15 domain, which binds the mRNA 5′ m7G cap and oligopyrimidine (TOP) motifs [2, 8]. Functionally, LARP1 regulates the stability, localization, and translation of TOP mRNAs downstream of mTORC1 signaling [9-12]. TOP mRNAs encode translation machinery components, such as ribosomal proteins and factors. LARP1 is directly phosphorylated by the mTOR kinase [13-17]. LARP1 also interacts with a large number of mRNAs in mTOR-independent pathways and has been implicated in cancer [18-23].

The LaM and RRM domains of LARP3, LARP4, LARP6, and LARP7 and the LaM domain of LARP1 have been structurally characterized [7, 24-33]. In LARP3, the LaM and RRM domains form a synergistic RNA-binding scaffold to bind uridylate oligonucleotides. The 3′-terminal uridylate binds to the LaM domain and the 3′ penultimate nucleotide interacts with a V-shaped clamp formed between the LaM and RRM domains [25, 26]. In contrast, the LARP1 LaM binds RNA as a stand-alone domain with a preference for poly(A) sequences [7]. The terminal and penultimate adenylate nucleotides (numbered -1 and -2 from the 3′-end) bind in the same way as uridylates in other LARP proteins but without contacts from an adjacent RRM domain. The terminal (-1) ribose is positioned by polar contacts with Asp346 and the adenine ring stacks on Phe348. The penultimate (-2) adenine ring stacks on Tyr336 and is positioned by a hydrogen bond with Gln333. Considerable variability was observed in the positions of the preceding nucleotides with either the (-3) or (-4) nucleotide stacking between His368 and the (-1) adenine.

LARP1 has been linked to protection of poly(A) from deadenylation and associated mRNA stabilization [2, 7, 34, 35]. Consistent with its association with PABP, LARP1 from human cell extracts immunoprecipitates with poly(A) RNA, but not with poly(U), poly(C), or poly(G) [36]. Assays in human HEK293 cells deleted of endogenous LARP1 (KO) showed that expression of LARP1 led to net lengthening of mRNA poly(A) tails which was attributed to protection from binding to the LaM domain [7, 37]. LARP1 in complex with PABPC1 was found preferentially associated with short tails and its depletion resulted in their accelerated deadenylation [35].

In the present study, we show that isolated guanosine residues in poly(A) sequences improve binding to the LaM domain of LARP1. High-resolution crystal structures of LARP1 LaM with six different RNAs: A_5G, A_4GA, A_3GA_2, U_6, and (R_P)- and (S_P)-diastereomers of a phosphorothioate derivative reveal the molecular interactions that allow for plasticity in base recognition while maintaining specificity for the RNA 3′-end. The increased affinity of the LARP1 LaM domain for poly(A) sequences containing single guanine residues suggests that in vivo LARP1 should be enriched on guanylated mixed-tailed mRNAs.

RESULTS

NMR studies with single nucleotides expose binding preference for guanine

We carried out NMR titrations with single nucleotides binding to ^{15}N-labeled LARP1 LaM to isolate the individual nucleotide interactions (Fig. 1A). The addition of nucleotides caused spectral changes similar to those observed with the hexamer A_6 but with smaller shifts and fewer signals affected (Suppl. Fig. S1) [7]. Unlike A_6, which showed NMR signals in slow exchange, the nucleotide titrations displayed fast exchange kinetics and significant broadening of some signals. The signals with the largest changes were the amide of Ile364 and side chain amides of Gln333.

Unexpectedly, 5′-GMP showed larger chemical shift changes than 5′-AMP (Fig. 1B). At 200 μM, 5′-GMP shifted the Gln333 signal twice as much as 5′-AMP. Both purines nucleotides bound better (showed larger shifts) than the pyrimidines 5′-UMP and 5′-CMP. We used the size of the chemical shift change as a function of nucleotide concentration to estimate binding affinities (Fig. 1C). As the protein

concentration is comparable to the binding affinity, fitting the changes required accounting for bound ligand when calculating the free ligand concentration. This had the advantage that it also provided an estimate of the binding stoichiometry. For 5′-GMP, the stoichiometry was measured to be 2.04 with an affinity of 40 μM. For 5′-AMP, the stoichiometry could not be determined but the K_d was measured to be 130 μM assuming a stoichiometry of 2. This is at odds with the affinities of oligonucleotides measured by isothermal titration calorimetry (ITC) [7]. The analysis of 22 different RNA oligonucleotides identified poly(A) RNA as the preferred ligand: A_6 bound with 14-fold better affinity than G_6, 11-fold better than U_6, and 200-fold better than C_6.

In addition to base specificity, the LaM domain is strongly selective for RNA with a 3′-hydroxyl. ITC experiments show that addition of a 3′-phosphate to A_6 decreases the binding affinity 200-fold [7]. The NMR experiments showed good agreement: the shift of the Ile364 peak with 3′-AMP shift was 30-fold smaller than with 5′-AMP (Fig. 1B). Titrations with 3′,5′-ADP and adenosine confirmed the roles of the 3′-hydroxyl and 5′-phosphate, respectively.

Comparison of the shifts of Ile364 and Gln333 suggests that they reflect distinct nucleotide binding sites. For several ligands, the size of chemical shift changes for Ile364 and Gln333 differed markedly. Ile364 was not appreciably shifted by 3′-AMP while Gln333 was. Similarly, doubly charged 3′,5′-ADP induced a small shift in Ile364 but broadened the Gln333 signal beyond detection. In crystal structures, the Gln333 side chain makes a hydrogen bond with the base in the (-2) position which suggests the NMR shift primarily reflects occupancy at that position. The amide of Ile364 sits under Phe367 near the binding site of the (-1) nucleotide and likely reports on the occupancy of that site. This interpretation rationalizes the differences in ligand sensitivity. Ile364 is extremely sensitive to modification of the 3′-hydroxyl since it reflects binding of the 3′-terminal nucleotide, while Gln333 tolerates a 3′-phosphate. Conversely, Gln333 is involved in the extensive contacts with the (-2) nucleotide base and shows strong base selectivity, while Ile364 shows shifts of more equal size for all four nucleotide bases.

Guanine improves RNA binding

We used isothermal titration calorimetry (ITC) experiments to probe the effect of guanine bases on RNA oligomer binding (Fig. 2, Suppl. Table S1, Suppl. Fig. S2). As previously reported, the LARP1 LaM domain bound the hexamer A_6 with 250 nM affinity. Single guanine substitutions markedly improved binding with AAAAGA showing the highest affinity, 80 nM, a 3-fold improvement over A_6. Substitutions at the (-1) and (-3) positions showed slightly smaller, approximately 2-fold increases. We also tested the effect of multiple guanine substitutions. Surprisingly, a second guanine base did not improve binding and, in some cases, decreased the affinity. For example, the doubly substituted hexamer AAAGAG bound with essentially the same affinity as AAAGAA and AAAAAG, while AAAAGG bound with half the affinity of AAAAGA.

Previous ITC experiments measured an affinity of 3.3 μM for G_6 binding to LaM, which is 40-fold weaker than AAAAGA. To explain the stark difference in affinity of single and all guanine RNAs, we examined the binding affinity of the dinucleotide GG by ITC. Injections of GG RNA into LaM generated a complex thermogram inconsistent with a single binding reaction (Fig. 3). Given the propensity of guanine oligonucleotides to form quadruplexes [38], we suspected that the complex thermogram arose from the presence of two processes: i) dissociation of quadruplexes of GG present in the concentrated solution in the syringe, and ii) binding of the single-stranded GG to the LaM domain. To test this, we reversed the concentrations of the components, injecting concentrated LaM into a 20-fold diluted solution of the RNA dinucleotide. This resulted in a normal thermogram which could be fit as a simple bimolecular interaction with 2.8 μM affinity. As a control, an ITC experiment with AG carried out in the standard manner measured an affinity of 3.1 μM, confirming the unusual titration behavior was specific to GG. As the stability of guanine quadruplexes increases with the number of guanines, these results explain the low affinity of G_6 relative to A_6 and the RNAs with only one or two guanine bases. Competition between quadruplex formation and LaM-binding decreases the apparent affinity of guanine-rich RNAs for the LARP1 LaM.

Structural determinants of base specificity

We turned to X-ray crystallography to understand the molecular basis of LARP1 preference for RNA with guanine substitutions (Table 1, Fig. 3). Co-crystallization trials of LARP1 (323-410) with the RNA hexamers, AAAAAG, AAAAGA, and AAAGAA, yielded crystals diffracting to better than 2 Å (Suppl. Table S2). We also crystallized the protein with RNA with uracil bases, U_6, and the Rp and Sp-diastereomers of a phosphorothioate derivative of A_6. The crystals were solved using molecular replacement with the structure of the unliganded LaM domain [7]. All structures showed clear, well-resolved electron density for the protein and 3′-terminal nucleotides (Suppl. Fig. S3).

Not surprisingly, the structures globally resemble the LARP1 LaM domain with bound poly(A) ligands [7]. We previously showed that RNAs can bind in two conformations that differ in the stacking of either the (-3) or (-4) adenine onto adenine (-1). In all the poly(A) structures, the 3′-terminal nucleotides are bound by a pocket formed by alpha helices α1, α2, and α4 (Fig. 3A). Nucleotides (-1) and (-2) are rigidly positioned by hydrogen bonds between the terminal ribose and Asp346, the helical dipole from alpha helix α4, and base stacking with Phe348 and Tyr336. In contrast, the (-3/-4) nucleotide is loosely positioned with large variations between the different structures (Fig. 3B). In the A_6 structure, the (-4) adenine stacks on His368 while the (-3) nucleotide is completely disordered (Fig. 3C). Comparison of the AAAAAG structure with A_6 shows the substituted guanine base is shifted to improve the stacking with Phe348 (Fig. 3D). The guanine N2 atom additionally forms an indirect hydrogen bond with the side chain of Arg351. In the crystal, this is formed via a sulfate ion in the crystallization buffer but could be formed via a water molecule observed in the A_4 structure [7].

The AAAAGA structure clearly explains the 3-fold improvement in binding affinity over A_6 (Fig. 3E). The introduction of a guanine base adds a hydrogen bond with Gln333. This is consistent with the broadening of the Gln333 side chain NMR resonances observed in the presence of 5′-GMP (Fig. 1A). Previous mutagenesis of Gln333 confirmed that it plays an oversized role in RNA binding with a 20-fold drop in affinity measured for the alanine substitution [7]. mRNA stabilization assays and poly(A) tail-

sequencing validated the requirement for Gln333 for LARP1 function in cells. We tested the effects of mutating Gln333 to alanine for binding guanylated poly(A) RNAs. ITC measurements confirmed that loss of the glutamine led to more than a 50-fold loss in binding affinity (Suppl. Table S3).

We also obtained a crystal structure with AAAGAA bound. Unlike the other structures, AAAGAA does not show notable differences relative to the A_6 structure (Suppl. Fig. S4A). The guanine base does not directly interact with the protein and the conformation of the bound adenine nucleotides is unchanged. Instead, the guanine base (-3) stacks on the 5′-terminal adenine (-6) and makes hydrogen bonds with its own phosphates and those of adenylate (-5). The structure is unusual in that all six nucleosides are visible in the electron density map due to crystal packing and contacts between the RNA 5′-terminal nucleotides (Suppl. Fig S4B).

To understand why the LARP1 LaM binds poly(U) weakly compared to other LARP proteins, we crystalized the domain with U_6 RNA and determined its structure at 1.30 Å resolution. U_6 binds LaM with 11 times lower affinity than A_6 [7]. In the structure, the key binding determinants are conserved although U_6 adopts the alternative base stacking conformation (-3/-1) with the third nucleotide stacked between the side chain of His368 and uracil (-1). Both (-3/-1) and (-4/-1) stacking configurations likely occur in solution. The crystal structure shows the ribose of nucleotide (-1) is rigidly positioned in the binding pocket formed by Asp346. Uracil bases (-1) and (-2) occupy the same positions as adenines (-1) and (-2) in the poly(A) structure (Fig. 3F). Uracil (-1) stacks on Phe348 and uracil (-2) stacks on Tyr336 with a hydrogen bond to Arg333 [7]. The uracil ring (-3) makes a single hydrogen bond to the protein, between O2 and the backbone amide of His368, compared to two for adenine (-4) in A_6. Density was observed for the ribose of uridiylate (-4) but it makes no contacts with the protein. Thus, the weaker stacking interactions and fewer protein contacts likely explain the lower affinity of U_6 compared to A_6.

Structural determinants of specificity for phosphoribose

Previous studies have demonstrated the importance of Asp346 and the equivalent aspartic acid in other LARP proteins for RNA binding [7, 24-31]. Conversely, modifications of the 3′ sugar demonstrated

the LARP1 LaM is strictly specific for the 3′-terminus. While a deoxyribose sugar is tolerated, blocking of the 3′-terminus with either a 2′-O-methyl or 3′-phosphate group completely prevents binding.[6] This strict specificity is thought to be a consequence of the tight positioning of phosphoribose in the LaM binding pocket.

To test the importance of the phosphate group, we prepared A_6 with phosphorothioate modifications at the 3′-terminal nucleotide (-1) and determined the structures of their complexes with LaM at 1.2 Å (Fig. 5). The (R_P)-diastereomer has the sulfur positioned above the binding pocket and reproduces the hydrogen bonding and other contacts seen with A_6 (Fig. 5A). The phosphate oxygen hydrogen bonds with both the backbone amide of Arg369 and the side chain OH of Tyr337. This positions the 3′-terminal ribose with its hydrophobic face (the face opposite the 2′- and 3′-OH groups) in close contact with the benzyl ring of Phe367. In agreement with the crystal structure, the R_P isomer binds with essentially the same affinity as A_6 (290 nM). The (S_P)-diastereomer switches the positions of the oxygen and sulfur in the phosphothioate group and has a dramatic effect on LaM binding. The low electronegativity of sulfur atom makes it a weak hydrogen bonding acceptor [39] and its larger atomic radius displaces the ribose away from Phe367 (Fig. 5C). ITC measurements showed the S_P isomer binds with 17 μM affinity, confirming the binding selectivity for the R_P isomer (Fig. 5D).

DISCUSSION

LARP proteins are named after the La autoantigen protein (subsequentially renamed LARP3). The family of proteins emerged early in evolution and are present in essentially all eukaryotes [3, 4]. The prototypical LARP gene underwent multiple duplication events to generate specialized isoforms that are conserved across species. It likely contained both LaM and RRM domains since the pair is present in most present day LARP proteins with a few notable exceptions, such as LARP1 [7, 40].

Human LARP1 is large protein (1019 or 1096 amino acids depending on the isoform) with only two independently folding domains. Together, they compose about a quarter of the protein: the LaM domain recognizes RNA 3′-termini and DM15, an alpha-helical HEAT-repeat domain, binds the mRNA 5′-cap and

TOP RNA sequences. DM15 domains are unique to LARP1 and LARP1B and serve to negatively regulate TOP mRNA translation in response to mTORC1 inhibition [8, 13, 16, 20, 21, 41]. Unlike the other LARP proteins which contain an RRM domain, the LARP1 LaM domain functions as a stand-alone RNA-binding domain with specificity for poly(A) RNA [7]. While the isolated LaM domain is sufficient for poly(A) binding, the regions adjacent to the La domain also contribute to RNA binding. Al-Ashtal and colleagues [15] observed that LARP1 residues 310–540 bound poly(A) RNA with 40 nM affinity, roughly 6-fold better than the isolated La domain. The LARP1 arginine-glycine (RG) repeat region (residues 250–267 in the 1019-residue isoform) also contributes to RNA binding. Mattijssen et al. [37] showed that a LARP1 fragment including this region exhibited different binding and functional properties. Ogami et al. [34] similarly showed the poly(A) tail lengthening function of LARP1 was less efficient in the absence of residues 249–311. The importance of intrinsically disordered regions was also observed in LARP4 and shown to be primarily responsible for RNA binding [30]. LARP1 also contains a PABP-interaction motif (PAM2) immediately following the LaM domain that serves to recruit PABPC1 and provides increased affinity and specificity for poly(A) mRNA [13, 21, 37]. Uniquely among LARP proteins, LARP1 has the potential to circularize mRNAs through binding of the mRNA 5´-cap by its DM15 domain and the 3'-end by the LaM domain.

Numerous studies have shown that, in addition to regulating TOP mRNA translation, LARP1 protects mRNA with poly(A) tails from degradation [7, 9, 10, 13, 35, 37, 42]. Of particular interest, is the observation that the incorporation of guanine bases (guanylation) into mRNA poly(A) tails shields them from rapid deadenylation [43, 44]. This was interpreted as arising from slowed deadenylation by CCR4-NOT but our observation of the enhanced affinity of guanine-containing poly(A) sequences suggests the preferential binding of the LaM domain to guanylated poly(A) tails contributes to their stability. Fittingly, LARP1 interacts with non-canonical poly(A) polymerases PAPD7 (TENT4A) and PAPD5 (TENT4B) to induce post-transcriptional polyadenylation of TOP mRNAs [34] and, together with PABPC1, LARP1 acts as barricade to deadenylation by the CCR4-NOT complex [35]. PAPD7 and PAPD5 are the same polymerases responsible for producing guanylated poly(A) tails [44]. Curiously, while guanylation of many

TOP mRNAs was observed, as a class, they were less frequently guanylated than average. mRNAs for secreted and endoplasmic reticulum proteins showed more guanylation than those of ribosomal proteins and translation factors [44]. This could reflect the absence of the metabolic signalling that triggers the accumulation and poly(A) tail lengthening of TOP mRNAs. Alternatively, it may reflect the mTOR independent functions of LARP1 in cancer cell lines where TOP mRNAs account for less than 4% of mRNAs bound by LARP1 [14, 18, 19].

The observation of 2 to 3-fold increased affinity for single guanine-containing RNAs led to the expectation that multiple guanine bases would further increase the affinity (Fig. 2B). Instead, there is no improvement and, in the case of the ligands AAAAGA (80 nM) and AAAAGG (140 nM), the second guanine leads to a loss of affinity. Similar behavior was observed with the dinucleotides AG and GG which both bind with ~3 μM affinity (Fig. 3). The biophysical basis for the negative cooperativity of the guanines is unclear. In general, relatively small (two-fold) differences in binding affinities are difficult to rationalize based on static crystal structures. The crystal structure of AAAGAA bound to the LaM does little to explain the 1.8-fold improvement in affinity. While comparison of the A_6 and AAAGAA complexes shows a small shift in the position of the (-3) adenine ring (Suppl. Fig. S4A), RNA bases at that position are highly variable (Fig. 3B) and the observed shift is unlikely to be fully responsible for the improved affinity. As an alternative explanation, in solution, the guanine base may bind in the (-3/-1) conformation with better stacking and hydrogen bonding interactions than the adenine base. In our study of poly(A) structures, we observed considerable variability in the stacking configurations (-3/-1 versus -4/-1). In one case the same RNA different crystals bound in two different configurations [7]. Multiple conformations are likely to exist in solution. Finally, comparison of the affinity different RNA sequences assumes that the free energies of the unbound RNAs are the same. This is clearly not the case for all guanine RNAs (G_2 and G_6), which can form guanine quadruplexes in competition with LaM binding. Uniquely, in the AAAGAA complex, the 5´-nucleotides make intra-RNA contacts and are visible in the electron density map (Suppl. Fig. S4B).

The crystal structure of U_6 complex does a better job explaining the lower affinity which results from fewer hydrogen bonds and smaller stacking interfaces. U_6 bound to the LaM domain in a -3/-1 stacking

conformation which is consistent with the structure reported for 3′-end poly(U) sequences interacting with LARP3 [26]. In LARP3, the La-module (the combination of LaM and RRM domains) binds the UUU 3′ termini of nascent RNA polymerase III transcripts, most of which are precursors to the tRNAs, protecting them from untimely digestion by 3′ exonucleases while also assisting their folding [25, 45, 46]. The U_6 structure underlines the plasticity in RNA recognition by the LARP1 LaM domain, which lacks the intermolecular contacts and binding specificity provided by the RRM domain found in other LARPs.

Ultimately, the key function of LaM domains appears to be the recognition of the RNA 3′-terminus. This is dramatically illustrated by the comparison of the NMR chemical shift changes from 3′-AMP and 5′-AMP (Fig. 1A). Moving the phosphate to the 3′ carbon completely eliminated binding adjacent to I364. The effect is much larger than base modifications. While the role of Asp346 in recognizing the 3′-hydroxyl was known, the importance of contacts between the (-1) phosphate and helix α4 had not been tested previously. We took advantage of chiral phosphorothioate derivatives to demonstrate the helix dipole and hydrogen bonds to backbone amides are major contributors to binding affinity. The strong chiral selectivity we observed opens the door to controlling the stability of synthetic RNAs through stereoselective phosphorothioate derivatives [47, 48].

MATERIALS AND METHODS

Expression and purification of proteins

The plasmid expressing human LARP1 LaM domain (residues 323-410) and its purification as a His-tag fusion protein from *E. coli* cells were described previously [7]. Amino acids are numbered according to the shorter 1019-residue isoform.

RNA oligonucleotides

RNA oligonucleotides A_6 (5′-$A_PA_PA_PA_PA_PA_P$A-3′), A_5G (5′-$A_PA_PA_PA_PA_PA_P$G-3′), A_4GA (5′-$A_PA_PA_PA_PG_PA_P$A-3′), and A_3GA_2 (5′-$A_PA_PA_PG_PA_P$A-3′) were synthesized on 2 × 2 μmol scale using an ABI 3400 DNA synthesizer employing the β-cyanoethylphosphoramidite method with long chain alkylamine

controlled pore glass (LCAA-CPG, 500 Å) as the solid support functionalized with a protected 5′-O-dimethoxytrityl ribonucleoside. Hexamers containing a phosphorothioate (thiophosphate) internucleotide linkage between the terminal 3′ adenylate residues (5′-$A_PA_PA_PA_PA_{PS}$A-3′) were prepared using the sulfurization reagent 3-phenyl 1,2,4-dithiazoline-5-one (PolyOrg Inc.) at a concentration of 0.1 M in acetonitrile and 2 equivalents of pyridine for a total exposure of 2 min after the coupling of the first β-cyanoethylphosphoramidite in the synthesis cycle. After this step, solid-phase synthesis proceeded according to previously published procedures [49]. Oligonucleotides were cleaved from the solid support, deprotected, purified by either preparatory denaturing PAGE or ion-exchange HPLC (for the separation of the (R_P)- and (S_P)-diastereomers of 5′-$A_PA_PA_PA_PA_{PS}$A-3′), and then desalted using C-18 SEP PAK cartridges. The dinucleotides, 5′-A_PG-3′ and 5′-G_PG-3′, were obtained from Jena Bioscience (Thuringia, Germany). U_6 (5′-$U_PU_PU_PU_PU_PU_P$U-3′) was obtained from Integrated DNA Technologies (Coralville, USA) and used without additional purification.

NMR spectroscopy

NMR samples were exchanged into 10 mM MES pH 6.3, 100 mM NaCl, 1 mM TCEP. For NMR titrations, nucleotides were added to 0.1 mM ^{15}N-labeled LARP1 (323-410) to final molar ratios of 5:1. All NMR experiments were performed at 25 ºC using a Bruker 600 MHz spectrometer. NMR spectra were processed using NMRPipe [50] and analyzed with SPARKY [51]. Binding affinities were measured by fitting the observed chemical shift changes accounting for bound ligand with a stoichiometry of two nucleotide binding sites. The chemical shifts and fitting formula and parameters are provided in a supplementary worksheet.

Isothermal titration calorimetry

ITC experiments were performed on the VP-ITC titration calorimeter (Malvern Instruments Ltd) except where noted. The syringe was loaded with 300 μM RNA sample, while the sample cell contained 20-30 μM LARP1 (323-410) sample. All experiments were carried out at 20 ºC with 29 injections of 10 μl.

Results were analyzed using ORIGIN software (MicroCal) and fitted to a binding model with a single set of identical sites.

Crystallization

Initial crystallization conditions were identified utilizing hanging drop vapor diffusion with the Classics II and Nucleix screens (QIAGEN). The best LARP1 LaM domain/RNA complex crystals were obtained by equilibrating a 0.6 µL drop of the LaM domain (residues 323-410) with oligonucleotide in a 1:1.1 molar ratio (10 mg/mL of protein) in buffer (10 mM MES pH 6.3, 100 mM NaCl), mixed with 0.6 µL of reservoir solution containing [0.1 M Bis-Tris pH 6.5, 2 M ammonium sulfate] for A_5G, [0.2 M ammonium acetate, 0.1 M Bis-Tris pH 6.5, 25% (w/v) PEG 3350] for A_4GA, [0.056 M sodium phosphate, 1.344 M potassium phosphate] for A_3GA_2, [0.2 M ammonium acetate, 0.1 M Bis-Tris pH 5.5, 25% (w/v) PEG 3350] for U_6, [0.1 M ammonium acetate, 0.1 M Bis-Tris pH 5.5, 17% (w/v) PEG 10000] for (R_P)-$A_PA_PA_PA_PA_{PS}A$, [0.1 M Bis-Tris pH 6.5, 28% (w/v) PEG 2000 MME] for (S_P)-$A_PA_PA_PA_PA_{PS}A$. Crystals grew in 3-14 days at 20 ºC. For data collection, crystals were cryo-protected by soaking in the reservoir solution supplemented with 30% (v/v) ethylene glycol for conditions PEG or otherwise with 25% glycerol.

Structure solution and refinement

Diffraction data from single crystals of LARP1 LaM domain and its RNA complexes were collected at the Canadian Light Source (CLS) and Cornell High-Energy Synchrotron Source (CHESS). Data processing and scaling were performed with HKL2000 [52]. The initial phases for the complex structures were determined by molecular replacement with Phaser [53], using the coordinates of the LARP1 LaM domain (PDB entry 7SOO) [7]. The starting protein model was then completed and adjusted with the program Coot [54] and improved by several cycles of refinement, using the program phenix.refine [55] and model refitting. The resulting electron density maps revealed clear density for each RNA oligonucleotide, which were manually built with the program Coot [54]. At the latest stage of refinement, we also applied

the translation-libration-screw (TLS) option [56]. The final models have all residues in the allowed regions of Ramachandran plot. Data collection and refinement statistics are given in Suppl. Table S2.

ACKNOWLEDGEMENTS

Crystallographic data were acquired at the Canadian Light Source (CLS) and the Cornell High-Energy Synchrotron Source (CHESS) Macromolecular Diffraction facility. CLS is supported by the Canada Foundation for Innovation, the Natural Sciences and Engineering Research Council, the National Research Council, the Canadian Institutes of Health Research, and the Government of Saskatchewan. CHESS is supported by National Science Foundation award DMR-0225180 and National Institutes of Health/NCRR award RR-01646. The study has been supported by funding from Canadian Institutes of Health Research grant FDN 159903 to K.G.

DATA AVAILABILITY

The authors confirm that the crystallographic data are available from the Protein Data Bank (PDB) under accession codes 8EY6 (A_5G), 8EY8 (A_4GA), 8EY7 (A_3GA_2), 8G91 (A_6 with R_P-phosphorothioate diastereomer), 8G90 (A_6 with S_P- phosphorothioate diastereomer), and 7SOW (U_6). Other data supporting the findings of this study are available within the article and its supplementary materials.

DISCLOSURE STATEMENT

The authors confirm that there are no relevant financial or non-financial competing interests to report.

REFERENCES

1. Bayfield, M.A., R. Yang, and R.J. Maraia, *Conserved and divergent features of the structure and function of La and La-related proteins (LARPs).* Biochim Biophys Acta, 2010. **1799**(5-6): p. 365-78.

2. Mattijssen, S., G. Kozlov, B.D. Fonseca, K. Gehring, and R.J. Maraia, *LARP1 and LARP4: up close with PABP for mRNA 3' poly(A) protection and stabilization.* RNA Biol, 2021. **18**(2): p. 259-274.

3. Bousquet-Antonelli, C. and J.M. Deragon, *A comprehensive analysis of the La-motif protein superfamily.* RNA, 2009. **15**(5): p. 750-64.

4. Deragon, J.M., *Distribution, organization an evolutionary history of La and LARPs in eukaryotes.* RNA Biol, 2021. **18**(2): p. 159-167.

5. Merret, R., L. Martino, C. Bousquet-Antonelli, S. Fneich, J. Descombin, E. Billey, M.R. Conte, and J.M. Deragon, *The association of a La module with the PABP-interacting motif PAM2 is a recurrent evolutionary process that led to the neofunctionalization of La-related proteins.* RNA, 2013. **19**(1): p. 36-50.

6. Maraia, R.J., S. Mattijssen, I. Cruz-Gallardo, and M.R. Conte, *The La and related RNA-binding proteins (LARPs): structures, functions, and evolving perspectives.* Wiley Interdiscip Rev RNA, 2017. **8**(6).

7. Kozlov, G., S. Mattijssen, J. Jiang, S. Nyandwi, T. Sprules, J.R. Iben, S.L. Coon, S. Gaidamakov, A.M. Noronha, C.J. Wilds, R.J. Maraia, and K. Gehring, *Structural basis of 3'-end poly(A) RNA recognition by LARP1.* Nucleic Acids Res, 2022. **50**(16): p. 9534-9547.

8. Lahr, R.M., B.D. Fonseca, G.E. Ciotti, H.A. Al-Ashtal, J.J. Jia, M.R. Niklaus, S.P. Blagden, T. Alain, and A.J. Berman, *La-related protein 1 (LARP1) binds the mRNA cap, blocking eIF4F assembly on TOP mRNAs.* Elife, 2017. **6**.

9. Schneider, C., F. Erhard, B. Binotti, A. Buchberger, J. Vogel, and U. Fischer, *An unusual mode of baseline translation adjusts cellular protein synthesis capacity to metabolic needs.* Cell Rep, 2022. **41**(2): p. 111467.

10. Fuentes, P., J. Pelletier, C. Martinez-Herraez, V. Diez-Obrero, F. Iannizzotto, T. Rubio, M. Garcia-Cajide, S. Menoyo, V. Moreno, R. Salazar, A. Tauler, and A. Gentilella, *The 40S-LARP1 complex reprograms the cellular translatome upon mTOR inhibition to preserve the protein synthetic capacity.* Sci Adv, 2021. **7**(48): p. eabg9275.

11. Philippe, L., A.M.G. van den Elzen, M.J. Watson, and C.C. Thoreen, *Global analysis of LARP1 translation targets reveals tunable and dynamic features of 5' TOP motifs.* Proc Natl Acad Sci U S A, 2020. **117**(10): p. 5319-5328.

12. Goering, R., A. Arora, M.C. Pockalny, and J.M. Taliaferro, *RNA localization mechanisms transcend cell morphology.* Elife, 2023. **12**.

13. Fonseca, B.D., C. Zakaria, J.J. Jia, T.E. Graber, Y. Svitkin, S. Tahmasebi, D. Healy, H.D. Hoang, J.M. Jensen, I.T. Diao, A. Lussier, C. Dajadian, N. Padmanabhan, W. Wang, E. Matta-Camacho, J. Hearnden, E.M. Smith, Y. Tsukumo, A. Yanagiya, M. Morita, E. Petroulakis, J.L. Gonzalez, G. Hernandez, T. Alain, and C.K. Damgaard, *La-related Protein 1 (LARP1) Represses Terminal Oligopyrimidine (TOP) mRNA Translation Downstream of mTOR Complex 1 (mTORC1).* J Biol Chem, 2015. **290**(26): p. 15996-6020.

14. Berman, A.J., C.C. Thoreen, Z. Dedeic, J. Chettle, P.P. Roux, and S.P. Blagden, *Controversies around the function of LARP1.* RNA Biol, 2021. **18**(2): p. 207-217.

15. Al-Ashtal, H.A., C.M. Rubottom, T.C. Leeper, and A.J. Berman, *The LARP1 La-Module recognizes both ends of TOP mRNAs.* RNA Biol, 2021. **18**(2): p. 248-258.

16. Philippe, L., J.J. Vasseur, F. Debart, and C.C. Thoreen, *La-related protein 1 (LARP1) repression of TOP mRNA translation is mediated through its cap-binding domain and controlled by an adjacent regulatory region.* Nucleic Acids Res, 2018. **46**(3): p. 1457-1469.

17. Jia, J.J., R.M. Lahr, M.T. Solgaard, B.J. Moraes, R. Pointet, A.D. Yang, G. Celucci, T.E. Graber, H.D. Hoang, M.R. Niklaus, I.A. Pena, A.K. Hollensen, E.M. Smith, M. Chaker-Margot, L. Anton, C. Dajadian, M. Livingstone, J. Hearnden, X.D. Wang, Y. Yu, T. Maier, C.K. Damgaard, A.J. Berman, T. Alain, and B.D. Fonseca, *mTORC1 promotes TOP mRNA translation through site-specific phosphorylation of LARP1.* Nucleic Acids Res, 2021. **49**(6): p. 3461-3489.

18. Mura, M., T.G. Hopkins, T. Michael, N. Abd-Latip, J. Weir, E. Aboagye, F. Mauri, C. Jameson, J. Sturge, H. Gabra, M. Bushell, A.E. Willis, E. Curry, and S.P. Blagden, *LARP1 post-transcriptionally regulates mTOR and contributes to cancer progression.* Oncogene, 2015. **34**(39): p. 5025-36.

19. Hopkins, T.G., M. Mura, H.A. Al-Ashtal, R.M. Lahr, N. Abd-Latip, K. Sweeney, H. Lu, J. Weir, M. El-Bahrawy, J.H. Steel, S. Ghaem-Maghami, E.O. Aboagye, A.J. Berman, and S.P. Blagden, *The RNA-binding protein LARP1 is a post-transcriptional regulator of survival and tumorigenesis in ovarian cancer.* Nucleic Acids Res, 2016. **44**(3): p. 1227-46.

20. Hong, S., M.A. Freeberg, T. Han, A. Kamath, Y. Yao, T. Fukuda, T. Suzuki, J.K. Kim, and K. Inoki, *LARP1 functions as a molecular switch for mTORC1-mediated translation of an essential class of mRNAs.* Elife, 2017. **6**.

21. Smith, E.M., N.E.H. Benbahouche, K. Morris, A. Wilczynska, S. Gillen, T. Schmidt, H.A. Meijer, R. Jukes-Jones, K. Cain, C. Jones, M. Stoneley, J.A. Waldron, C. Bell, B.D. Fonseca, S.

Blagden, A.E. Willis, and M. Bushell, *The mTOR regulated RNA-binding protein LARP1 requires PABPC1 for guided mRNA interaction.* Nucleic Acids Res, 2021. **49**(1): p. 458-478.

22. To, T.L., A.M. Cuadros, H. Shah, W.H.W. Hung, Y. Li, S.H. Kim, D.H.F. Rubin, R.H. Boe, S. Rath, J.K. Eaton, F. Piccioni, A. Goodale, Z. Kalani, J.G. Doench, D.E. Root, S.L. Schreiber, S.B. Vafai, and V.K. Mootha, *A Compendium of Genetic Modifiers of Mitochondrial Dysfunction Reveals Intra-organelle Buffering.* Cell, 2019. **179**(5): p. 1222-1238 e17.

23. Haneke, K., J. Schott, D. Lindner, A.K. Hollensen, C.K. Damgaard, C. Mongis, M. Knop, W. Palm, A. Ruggieri, and G. Stoecklin, *CDK1 couples proliferation with protein synthesis.* J Cell Biol, 2020. **219**(3).

24. Alfano, C., D. Sanfelice, J. Babon, G. Kelly, A. Jacks, S. Curry, and M.R. Conte, *Structural analysis of cooperative RNA binding by the La motif and central RRM domain of human La protein.* Nat Struct Mol Biol, 2004. **11**(4): p. 323-9.

25. Teplova, M., Y.R. Yuan, A.T. Phan, L. Malinina, S. Ilin, A. Teplov, and D.J. Patel, *Structural basis for recognition and sequestration of UUU(OH) 3' temini of nascent RNA polymerase III transcripts by La, a rheumatic disease autoantigen.* Mol Cell, 2006. **21**(1): p. 75-85.

26. Kotik-Kogan, O., E.R. Valentine, D. Sanfelice, M.R. Conte, and S. Curry, *Structural analysis reveals conformational plasticity in the recognition of RNA 3' ends by the human La protein.* Structure, 2008. **16**(6): p. 852-62.

27. Martino, L., S. Pennell, G. Kelly, B. Busi, P. Brown, R.A. Atkinson, N.J. Salisbury, Z.H. Ooi, K.W. See, S.J. Smerdon, C. Alfano, T.T. Bui, and M.R. Conte, *Synergic interplay of the La motif, RRM1 and the interdomain linker of LARP6 in the recognition of collagen mRNA expands the RNA binding repertoire of the La module.* Nucleic Acids Res, 2015. **43**(1): p. 645-60.

28. Eichhorn, C.D., R. Chug, and J. Feigon, *hLARP7 C-terminal domain contains an xRRM that binds the 3' hairpin of 7SK RNA.* Nucleic Acids Res, 2016. **44**(20): p. 9977-9989.

29. Eichhorn, C.D., Y. Yang, L. Repeta, and J. Feigon, *Structural basis for recognition of human 7SK long noncoding RNA by the La-related protein Larp7.* Proc Natl Acad Sci U S A, 2018. **115**(28): p. E6457-E6466.

30. Cruz-Gallardo, I., L. Martino, G. Kelly, R.A. Atkinson, R. Trotta, S. De Tito, P. Coleman, Z. Ahdash, Y. Gu, T.T.T. Bui, and M.R. Conte, *LARP4A recognizes polyA RNA via a novel binding mechanism mediated by disordered regions and involving the PAM2w motif, revealing interplay between PABP, LARP4A and mRNA.* Nucleic Acids Res, 2019. **47**(8): p. 4272-4291.

31. Yang, Y., S. Liu, S. Egloff, C.D. Eichhorn, T. Hadjian, J. Zhen, T. Kiss, Z.H. Zhou, and J. Feigon, *Structural basis of RNA conformational switching in the transcriptional regulator 7SK RNP.* Mol Cell, 2022. **82**(9): p. 1724-1736 e7.

32. Uchikawa, E., K.S. Natchiar, X. Han, F. Proux, P. Roblin, E. Zhang, A. Durand, B.P. Klaholz, and A.C. Dock-Bregeon, *Structural insight into the mechanism of stabilization of the 7SK small nuclear RNA by LARP7.* Nucleic Acids Res, 2015. **43**(6): p. 3373-88.

33. Lizarrondo, J., A.C. Dock-Bregeon, L. Martino, and M.R. Conte, *Structural dynamics in the La-module of La-related proteins.* RNA Biol, 2021. **18**(2): p. 194-206.

34. Ogami, K., Y. Oishi, K. Sakamoto, M. Okumura, R. Yamagishi, T. Inoue, M. Hibino, T. Nogimori, N. Yamaguchi, K. Furutachi, N. Hosoda, H. Inagaki, and S.I. Hoshino, *mTOR- and LARP1-dependent regulation of TOP mRNA poly(A) tail and ribosome loading.* Cell Rep, 2022. **41**(4): p. 111548.

35. Park, J., M. Kim, H. Yi, K. Baeg, Y. Choi, Y.S. Lee, J. Lim, and V.N. Kim, *Short poly(A) tails are protected from deadenylation by the LARP1-PABP complex.* Nat Struct Mol Biol, 2023. **30**(3): p. 330-338.

36. Aoki, K., S. Adachi, M. Homoto, H. Kusano, K. Koike, and T. Natsume, *LARP1 specifically recognizes the 3' terminus of poly(A) mRNA.* FEBS Lett, 2013. **587**(14): p. 2173-8.

37. Mattijssen, S., G. Kozlov, S. Gaidamakov, A. Ranjan, B.D. Fonseca, K. Gehring, and R.J. Maraia, *The isolated La-module of LARP1 mediates 3' poly(A) protection and mRNA stabilization, dependent on its intrinsic PAM2 binding to PABPC1.* RNA Biol, 2021. **18**(2): p. 275-289.

38. Rhodes, D. and H.J. Lipps, *G-quadruplexes and their regulatory roles in biology.* Nucleic Acids Res, 2015. **43**(18): p. 8627-37.

39. Zhang, Z., J. Vogele, K. Mrazikova, H. Kruse, X. Cang, J. Wohnert, M. Krepl, and J. Sponer, *Phosphorothioate Substitutions in RNA Structure Studied by Molecular Dynamics Simulations, QM/MM Calculations, and NMR Experiments.* J Phys Chem B, 2021. **125**(3): p. 825-840.

40. Kerkhofs, K., J. Garg, E. Fafard-Couture, S. Abou Elela, M.S. Scott, R.E. Pearlman, and M.A. Bayfield, *Altered tRNA processing is linked to a distinct and unusual La protein in Tetrahymena thermophila.* Nat Commun, 2022. **13**(1): p. 7332.

41. Cassidy, K.C., R.M. Lahr, J.C. Kaminsky, S. Mack, B.D. Fonseca, S.R. Das, A.J. Berman, and J.D. Durrant, *Capturing the Mechanism Underlying TOP mRNA Binding to LARP1.* Structure, 2019. **27**(12): p. 1771-1781 e5.

42. Gentilella, A., F.D. Moron-Duran, P. Fuentes, G. Zweig-Rocha, F. Riano-Canalias, J. Pelletier, M. Ruiz, G. Turon, J. Castano, A. Tauler, C. Bueno, P. Menendez, S.C. Kozma, and G. Thomas,

Autogenous Control of 5'TOP mRNA Stability by 40S Ribosomes. Mol Cell, 2017. **67**(1): p. 55-70 e4.

43. Chang, H., J. Lim, M. Ha, and V.N. Kim, *TAIL-seq: genome-wide determination of poly(A) tail length and 3' end modifications.* Mol Cell, 2014. **53**(6): p. 1044-52.

44. Lim, J., D. Kim, Y.S. Lee, M. Ha, M. Lee, J. Yeo, H. Chang, J. Song, K. Ahn, and V.N. Kim, *Mixed tailing by TENT4A and TENT4B shields mRNA from rapid deadenylation.* Science, 2018. **361**(6403): p. 701-704.

45. Yoo, C.J. and S.L. Wolin, *The yeast La protein is required for the 3' endonucleolytic cleavage that matures tRNA precursors.* Cell, 1997. **89**(3): p. 393-402.

46. Chakshusmathi, G., S.D. Kim, D.A. Rubinson, and S.L. Wolin, *A La protein requirement for efficient pre-tRNA folding.* EMBO J, 2003. **22**(24): p. 6562-72.

47. Jahns, H., N. Taneja, J.L.S. Willoughby, M. Akabane-Nakata, C.R. Brown, T. Nguyen, A. Bisbe, S. Matsuda, M. Hettinger, R.M. Manoharan, K.G. Rajeev, M.A. Maier, I. Zlatev, K. Charisse, M. Egli, and M. Manoharan, *Chirality matters: stereo-defined phosphorothioate linkages at the termini of small interfering RNAs improve pharmacology in vivo.* Nucleic Acids Res, 2022. **50**(3): p. 1221-1240.

48. Crooke, S.T., P.P. Seth, T.A. Vickers, and X.H. Liang, *The Interaction of Phosphorothioate-Containing RNA Targeted Drugs with Proteins Is a Critical Determinant of the Therapeutic Effects of These Agents.* J Am Chem Soc, 2020. **142**(35): p. 14754-14771.

49. Copp, W., A.Y. Denisov, J. Xie, A.M. Noronha, C. Liczner, N. Safaee, C.J. Wilds, and K. Gehring, *Influence of nucleotide modifications at the C2' position on the Hoogsteen base-paired parallel-stranded duplex of poly(A) RNA.* Nucleic Acids Res, 2017. **45**(17): p. 10321-10331.

50. Delaglio, F., S. Grzesiek, G.W. Vuister, G. Zhu, J. Pfeifer, and A. Bax, *NMRPipe: a multidimensional spectral processing system based on UNIX pipes.* J Biomol NMR, 1995. **6**(3): p. 277-93.

51. Goddard, T.D. and D.G. Kneller, *SPARKY 3.* University of California, San Francisco, 2008.

52. Otwinowski, Z. and W. Minor, *Processing of X-ray diffraction data collected in oscillation mode.* Methods Enzymol, 1997. **276**: p. 307-26.

53. McCoy, A.J., R.W. Grosse-Kunstleve, P.D. Adams, M.D. Winn, L.C. Storoni, and R.J. Read, *Phaser crystallographic software.* J Appl Crystallogr, 2007. **40**(Pt 4): p. 658-674.

54. Emsley, P. and K. Cowtan, *Coot: model-building tools for molecular graphics.* Acta Crystallogr D Biol Crystallogr, 2004. **60**(Pt 12 Pt 1): p. 2126-32.

55. Adams, P.D., P.V. Afonine, G. Bunkoczi, V.B. Chen, N. Echols, J.J. Headd, L.W. Hung, S. Jain, G.J. Kapral, R.W. Grosse Kunstleve, A.J. McCoy, N.W. Moriarty, R.D. Oeffner, R.J. Read, D.C. Richardson, J.S. Richardson, T.C. Terwilliger, and P.H. Zwart, *The Phenix software for automated determination of macromolecular structures.* Methods, 2011. **55**(1): p. 94-106.

56. Winn, M.D., G.N. Murshudov, and M.Z. Papiz, *Macromolecular TLS refinement in REFMAC at moderate resolutions.* Macromolecular Crystallography, Pt D, 2003. **374**: p. 300-321.

Table 1. X-ray crystal structures reported

RNA	Res., Å	PDB code
AAAAAG	1.63	8EY6
AAAAGA	1.30	8EY8
AAAGAA	1.35	8EY7
(*R*)-AAAAA$_{PS}$A	1.20	8G91
(S)-AAAAA$_{PS}$A	1.20	8G90
UUUUUU	1.30	7SOW

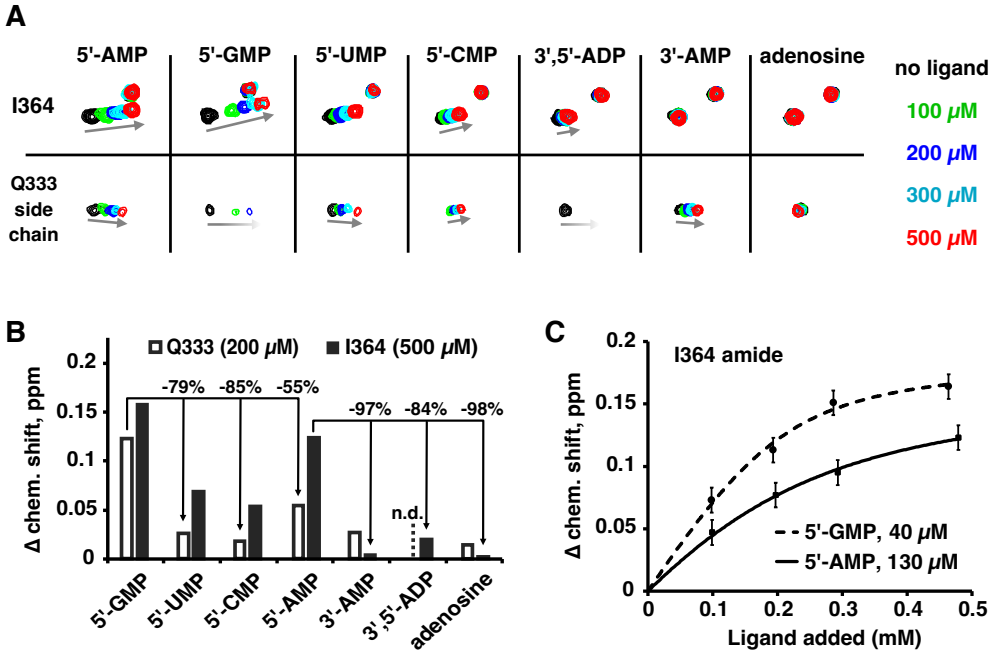

Figure 1. NMR reveals the LaM domain has distinct sites for mononucleotides with a preference for 5′-GMP. (A) Portions of ^{15}N-^{1}H correlation spectra of ^{15}N-labeled LARP1 (323-410) upon addition of nucleotides or adenosine. Nucleotides bearing 3′-phosphates only shifted the Q333 side chain signal while 5′-phosphonucleotides shifted both Q333 and I364. Full spectra are shown in Suppl. Fig. S1. (**B**) Plot of the magnitude of proton chemical shift changes shows 5′-GMP induced the largest chemical shift changes. n.d.= not determined. (**C**) Measurement of binding affinities for 5′-GMP and 5′-AMP.

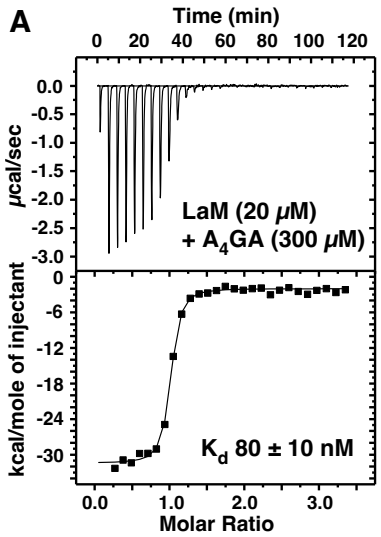

B

RNA	K_d, nM	Rel. aff.	ΔH, kcal mol^{-1}	ΔS, cal mol^{-1} K^{-1}
AAAAAA	250 ± 15	1.0	-19.9	-37.6
AAAAAG	130 ± 20	1.9	-27.5	-62.3
AAAAGA	80 ± 10	3.2	-29.5	-68.0
AAAGAA	140 ± 20	1.8	-27.7	-63.2
AAGAAA	140 ± 10	1.8	-29.3	-68.8
AAAAGG	140 ± 10	1.8	-27.4	-62.3
AAAGAG	120 ± 10	2.0	-31.2	-74.7
AAGAGA	70 ± 10	3.6	-38.3	-97.9

Figure 2. Isolated guanine bases increase the affinity of LaM binding measured by ITC. (A) Thermogram of the RNA ligand 5′-$A_PA_PA_PA_PG_PA$-3′ binding LARP1 (323-410). **(B)** Table of binding affinities of singly and doubly guanine-substituted poly(A) RNAs. Experimental details are given in Suppl. Table 1 and Suppl. Fig. S2.

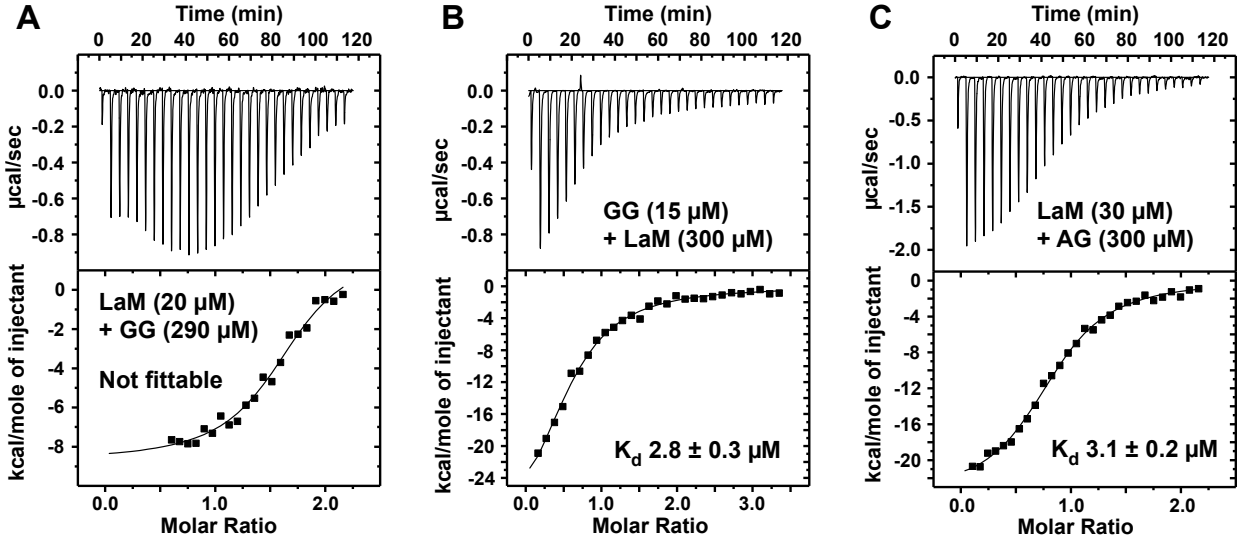

Figure 3. Guanine quadruplex formation competes with LaM binding. (A) ITC thermogram of concentrated 5′-A$_P$A-3′ injected into dilute LARP1 (323-410). The thermogram cannot be fit as simple intermolecular binding. **(B)** ITC thermogram with the syringe and cell components reversed shows the normal behavior for 1-to-1 intermolecular binding. **(C)** Control of concentrated 5′-A$_P$G-3′ injected into dilute LARP1 (323-410) shows normal binding.

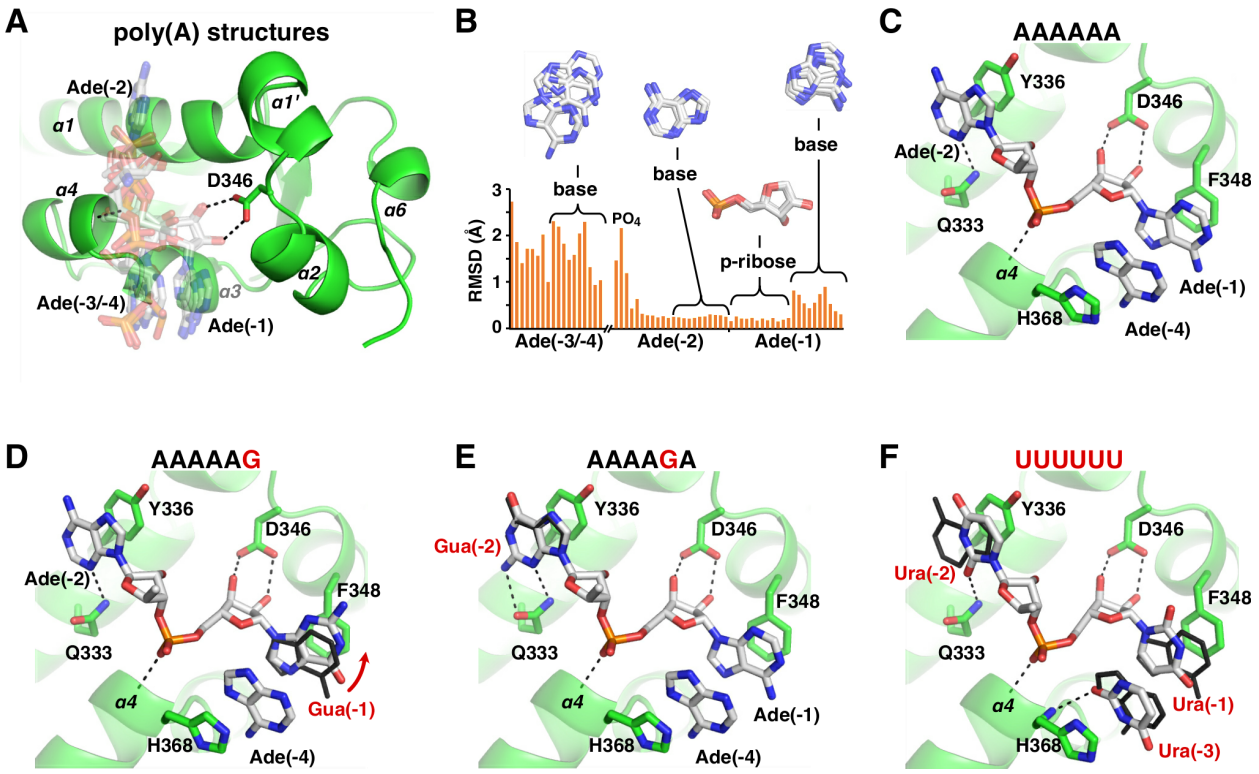

Figure 4. Structures of LARP1 LaM domain in complex with guanosine-containing poly(A) RNAs and poly(U). (A) Overlay of seven structures of poly(A) RNAs: 2×A_3, A_4, 2×A_6, A_3UA_2, and A_{11} [7]. Two different stacking conformations are present. In four structures, adenine (-4), numbered from the 3′-end, stacks on adenine (-1), while adenine (-3) does so in the other structures. Specificity for the 3′-terminus is mediated by polar contacts with Asp346. **(B)** Spread of atomic positions in the seven structures. Ribose (-1) and adenine (-2) show the least spread in the overlay. **(C)** Structure of A_6 bound to LARP1 LaM (PDB 7SOS) [7]. Adenine base (-1) and adenine (-4) stack between Phe348 and His368. Adenine (-2) stacks against Tyr336. (Only selected atoms are shown for clarity.) **(D)** Structure of the complex with A_5G. Guanine (-1) is shifted up relative to adenine in the A_6 structure (*black*). The guanine N2 makes an additional hydrogen bond with an ordered sulfate ion in the crystal (*not shown*). **(E)** Structure of the complex with A_4GA. Guanine base (-2) makes additional hydrogen bond with Gln333, improving the binding affinity. **(F)** Comparison of the complexes with U_6. The uracil bases overlap with adenines in the

A_6 structure (*black*) but are smaller and contribute less to the binding affinity. Adenine (-4) makes two hydrogen bonds with protein backbone atoms (*not shown*) while uracil (-3) makes only one.

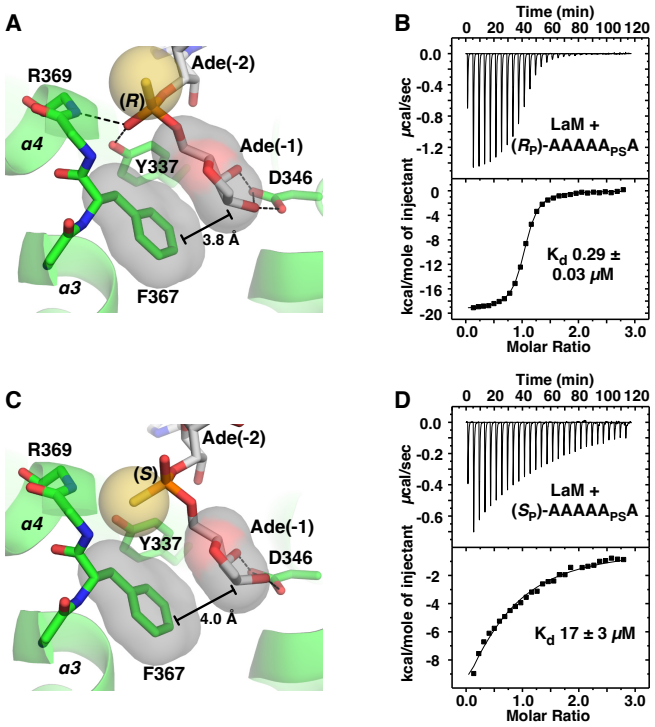

Figure 5. Structure of LARP1 LaM domain with phosphorothioate-containing A_6 RNA. (**A**) Crystal structure of the complex of the (R_P)-diastereomer 5′-$A_PA_PA_PA_PA_{PS}$A-3′ shows the sulfur atom (*yellow*) does not interfere with binding. As observed in structures with phosphate, the 3′-ribose is positioned by hydrogen bonds with Asp346 and packing of the sugar aliphatic face against Phe367. The phosphorothioate makes hydrogen bonds with the backbone amide of Arg369 and side chain hydroxyl of Tyr337. (**B**) ITC confirms the (R_P)-phosphorothioate does not affect binding. (**C**) Complex of (S_P)-diastereomer. The sulfur disrupts hydrogen bonds and shifts the ribose away from Phe367. (**D**) ITC shows the (S_P)-phosphorothioate binds with 60-fold lower affinity.